nature physics

LETTERS

PUBLISHED ONLINE: 6 JANUARY 2013 | DOI: 10.1038/NPHYS2516

How basin stability complements the linear-stability paradigm

Peter J. Menck[1,2]*, Jobst Heitzig[1], Norbert Marwan[1] and Jürgen Kurths[1,2,3]

The human brain[1,2], power grids[3], arrays of coupled lasers[4] and the Amazon rainforest[5,6] are all characterized by multistability[7]. The likelihood that these systems will remain in the most desirable of their many stable states depends on their stability against significant perturbations, particularly in a state space populated by undesirable states. Here we claim that the traditional linearization-based approach to stability is too local to adequately assess how stable a state is. Instead, we quantify it in terms of basin stability, a new measure related to the volume of the basin of attraction. Basin stability is non-local, nonlinear and easily applicable, even to high-dimensional systems. It provides a long-sought-after explanation for the surprisingly regular topologies[8–10] of neural networks and power grids, which have eluded theoretical description based solely on linear stability[11–13]. We anticipate that basin stability will provide a powerful tool for complex systems studies, including the assessment of multistable climatic tipping elements[14].

Complex systems science relies heavily on linear stability analysis, in which state of a dynamic system (more correctly, its dynamic regime) is assessed basically by inspecting the dominant curvature of the potential energy function in the state's surroundings (as expressed by Lyapunov exponents). The absolute value of the curvature measures the speed of convergence or divergence after a small perturbation, and its sign qualifies the state as stable or unstable. Such linearization-based considerations are inherently local; therefore, they are not sufficient to quantify how stable a state is against non-small perturbations. Quantification of stability in this sense requires a global concept: the basin of attraction $\mathcal{B}$ of a state is the set of initial points in state space from which the system converges to this state. Complete knowledge of the basin would allow us to fully assess the state's stability: one could classify perturbations into the permissible and the impermissible. See Fig. 1.

However, basins are intricate entities[15] and especially hard to explore in high dimensions. Here we therefore focus on a single but fundamental property: the basin's volume. The authors of ref. 16 interpret the volume of a state's basin of attraction as a measure of the likelihood of arrival at this state, that is, as a measure of the state's relevance. Almost equivalently, we understand the volume of the basin as an expression of the likelihood of return to the state after any random—possibly non-small—perturbation. This yields a second interpretation: the basin's volume quantifies how stable a state is. To the best of our knowledge, this interpretation has not yet been employed in complex systems science. We refer to the quantification of stability based on the basin's volume as basin stability $S_{\mathcal{B}}$.

For climatic tipping elements[14] it would be particularly useful to know how stable the desirable (that is, present) state is against perturbations. One such tipping element is the Amazon rainforest, which presumably possesses two stable states: the present fertile forest state and a barren savanna state[5,6]. A transition would emit huge amounts of carbon dioxide captured in the rich vegetation. Amazonian bistability arises from a positive feedback: deep-rooting trees take up water stored in the soil and transpire it to the atmosphere. Thereby, forest cover in an area increases overall precipitation and improves its own growing conditions. Consequently, a rather arid area (that is, an area with weak precipitation inflow) may still be supportive of forest growth if its forest cover exceeds a certain critical threshold; were forest cover pushed below this threshold, the area would lose all of its trees.

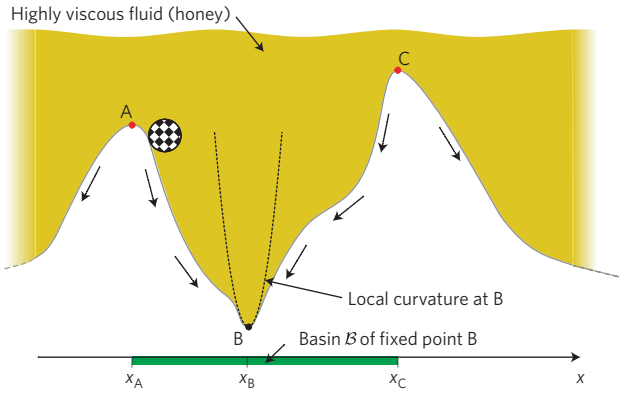

Figure 1 | Thought experiment: marble on a marble track. The track is immersed in a highly viscous fluid to make the system's state space one-dimensional. Dashed arrows indicate where the marble would roll from each position. A, B and C label fixed points. Only B is stable. The green bar indicates B's basin of attraction $\mathcal{B}$. If the marble is perturbed from B to a state within the basin, it will return to B. Such perturbations are permissible. Perturbations to states outside the basin are impermissible. The dashed parabola shows the local curvature around B, fitting the true marble track poorly in most of the basin.

This is summarized in a conceptual model (see Supplementary Information),

$$\frac{\mathrm{d}C}{\mathrm{d}t} = F(C) = \begin{cases} r(1-C)C - xC & \text{if } C > C_{\mathrm{crit}} \\ -xC & \text{if } C < C_{\mathrm{crit}} \end{cases}$$

Here, C is the relative forest cover that grows with the saturating rate r if $C > C_{\mathrm{crit}}$ and dies with rate x (assuming $r > x > 0$). C_{crit} is the critical forest cover threshold. This model has two equilibria, the forest state $C_{\mathrm{F}} = 1 - x/r$ and the savanna state $C_{\mathrm{S}} = 0$. The

[1]Research Domain on Transdisciplinary Concepts and Methods, Potsdam Institute for Climate Impact Research, PO Box 60 12 03, 14412 Potsdam, Germany, [2]Department of Physics, Humboldt University of Berlin, Newtonstraße 15, 12489 Berlin, Germany, [3]Institute for Complex Systems and Mathematical Biology, University of Aberdeen, Aberdeen AB24 3UE, UK. *e-mail: menck@pik-potsdam.de.

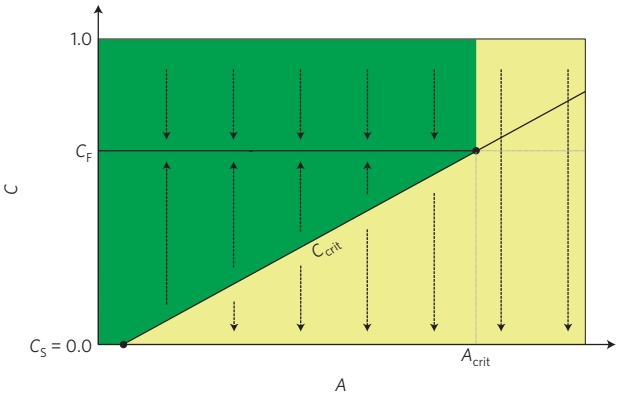

Figure 2 | State diagram of a bistable stylized forest–savanna model. Dashed arrows show where the system state, forest cover C, would move from a certain initial state at given aridity A. The green (light yellow) area is the basin of attraction of the forest (savanna) state C_F (C_S). Solid circles indicate the emergence or disappearance of an equilibrium.

equilibrium C_F (respectively, C_S) exists and is stable if $C_F > C_{crit}$ (respectively, $C_{crit} > 0$). Assuming that C_{crit} increases linearly with aridity A, we obtain the state diagram shown in Fig. 2.

Global warming may drive up aridity, pushing it eventually beyond the bifurcation point A_{crit} where the forest state vanishes. As aridity increases, the volume of the C_F state's basin of attraction shrinks, indicating that the forest state becomes less stable against perturbations. Indeed, owing to this reduced basin stability, a large perturbation such as strong deforestation might push the system to the savanna state long before aridity reaches A_{crit}. Crucially, none of this is reflected by linear stability, which judges the forest state C_F only by the stability coefficient $F'(C_F) = x - r$ that remains constant as aridity goes up.

This implies, first, that there is no critical slowing down. Indeed, linear early-warning signals[17] can be absent in systems with strong nonlinearities such as this model. Second, because of their highly local perspective, linear stability and hence the small-perturbation convergence rate do not indicate how stable C_F is against non-small perturbations. They are unreliable proxies, in contradiction to previous observations[17,18].

Note that both effects may also emerge in such simple mechanical systems as a damped driven pendulum (see Supplementary Information). Clearly, global stability concepts are needed.

Such global stability concepts could incorporate potential energy functions: deeper valleys would correspond to more stable states (Fig. 1). However, energy functions may not be available for many relevant (dissipative) systems. Furthermore, the estimation of energy levels on the basin boundary is numerically costly in high dimensions. An alternative approach was suggested, globally quantifying stability (or resilience, in the original nomenclature) in terms of the width of the basin of attraction in a particular direction[19,20]. This concept has inspired a host of studies on complex socioecological systems. Yet the measure of stability it implies "is not so easily quantified, even in models"[18]. One reason is that, in systems with many state variables, it is impossible to identify the single most relevant direction along which the width of the basin should be gauged. Our basin stability offers two important improvements: first, it follows a volume-based probabilistic approach that is compatible with the natural uncertainty about the strength and direction of perturbations; second, it provides a measure of stability that is clearly defined and easily quantified even in high-dimensional systems (see Methods).

Basin stability's applicability to high-dimensional systems allows us to tackle a puzzle that has long haunted complex networks science. Researchers in this field strive to understand how a network's topology serves its function and robustness[21,22]. Special effort has been put into multistable dynamic networks in which a synchronous state competes with alternative non-synchronous or partly synchronous states[11–13,23]. In a power grid, for instance, all components have to be operated at the same synchronous frequency to achieve steady power flows and to avoid damaging resonance effects[3]. In the brain, both neural communication[24] and memory processes[25,26] rely vitally on the synchronous firing of neurons. This means that, although synchronization is also associated with pathological states such as Parkinsonian tremor[27], the functional ability to support synchrony is as pivotal for the brain as it is for power grids. The problem with both kinds of network is that their real-world topologies look completely different from what the theory predicts.

The theory is as follows. If the synchronous state of a dynamic network is to be maintained, it must be stable against perturbations. A groundbreaking study[11] based on linearization revealed that, for a network of identical oscillators, the stability of the synchronous state can directly be inferred from the Laplacian, a matrix that reflects the coupling topology (see Supplementary Information). Indeed, for many types of oscillator, the synchronous state is stable if the ratio of the Laplacian's maximum and minimum non-zero eigenvalues, $R = \lambda_{max}/\lambda_{min}$, is smaller than an oscillator-specific stability threshold, $\beta = \alpha_2/\alpha_1$, provided the coupling strength is chosen from the stability interval, $I_s = (\alpha_1/\lambda_{min}, \alpha_2/\lambda_{max})$. The ratio R is known as the synchronizability of a network. Networks with smaller R are considered more synchronizable[12]. To determine what particularly synchronizable networks look like, researchers[13] employed the Watts–Strogatz graph generation model[8] and found that, as the model is tuned from regular lattices (model parameter $p = 0$) to random graphs ($p = 1$), synchronizability shows a strong, monotonical improvement (Fig. 3a).

Consequently, according to linear-stability-based synchronizability, real-world networks whose function relies on synchronization should ideally look like random graphs. However, neural networks and power grids exhibit small-world topologies that, from the Watts–Strogatz model's perspective, are far more regular than random graphs[8–10]. Indeed, when building well-functioning synchronizable networks, nature and civilization seem to shun the predicted randomness. This discrepancy between theory and observation has left networks research with a long-standing puzzle.

Attempting to complement the theory, we applied basin stability to ensembles of Watts–Strogatz networks consisting of paradigmatic Rössler oscillators, in which the dynamics at node i obey

$$\dot{x}_i = -y_i - z_i - K\sum_{j=1}^{N} L_{ij}x_j \quad (1)$$

$$\dot{y}_i = x_i + ay_i \quad (2)$$

$$\dot{z}_i = b + z_i(x_i - c) \quad (3)$$

with coupling constant K, Laplacian matrix L, $a = b = 0.2$, and $c = 7.0$. Every such network has a synchronous state in which all nodes follow the same trajectory. A network's synchronous state is stable if its synchronizability $R < \alpha_2/\alpha_1 = 37.85$ and $K \in I_s = (\alpha_1/\lambda_{min}, \alpha_2/\lambda_{max})$, where $\alpha_1 = 0.1232$ and $\alpha_2 = 4.663$. However, the level of R does not quantify how stable the synchronous state is against perturbations. To address this yet unasked question, for each network we estimated the synchronous state's basin stability S_B for several $K \in I_s$ and computed the mean $\bar{S}_B = \text{mean}\langle S_B(K)\rangle_{K\in I_s}$ (see Methods). Finally, we averaged $\bar{S}_B$ over the ensemble to obtain the expected basin stability $\langle\bar{S}_B\rangle$. We found that, in sharp contrast to synchronizability, expected basin stability declines exponentially fast as networks become more random (Fig. 3a,b; for a qualitative explanation, see Supplementary Information). Therefore, the synchronous state is much more stable in networks that are more regular.

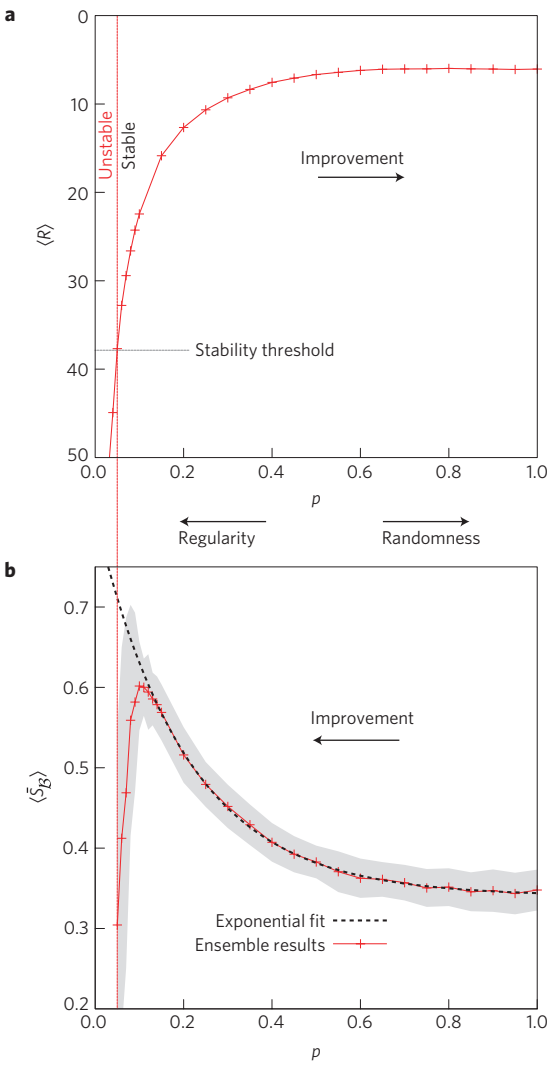

Figure 3 | Synchronizability and basin stability in Watts–Strogatz networks of chaotic oscillators. a, Expected synchronizability $\langle R\rangle$ versus the Watts–Strogatz model's parameter p. The scale of the y axis was reversed to indicate improvement on increase in p. **b**, Expected basin stability $\langle \bar{S}_{\mathcal{B}}\rangle$ versus p. The grey shading indicates $\pm$ one standard deviation. The dashed line shows an exponential curve fitted to the ensemble results for $p \geq 0.15$. Solid lines are guides to the eye. The plots shown were obtained for $N = 100$ oscillators of Rössler type, each having on average $k = 8$ neighbours. Choices of larger N and different k produce results that are qualitatively the same. See Methods and Supplementary Information for details and a qualitative explanation of the main characteristics.

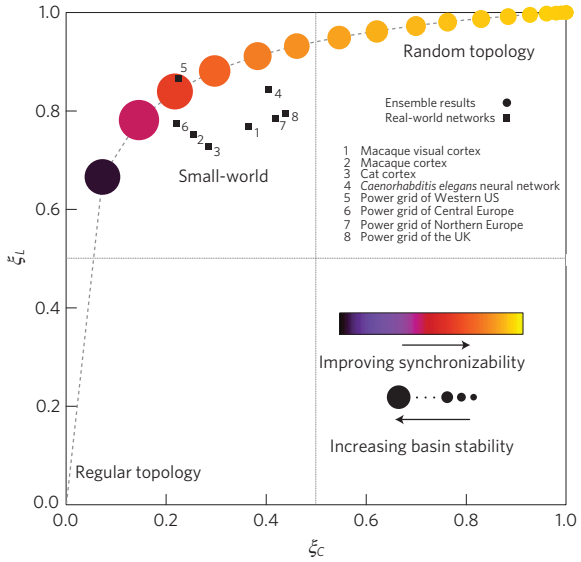

Figure 4 | Topological comparison of ensemble results with real-world networks. Circles represent the results for Watts–Strogatz networks with $N = 100$, $k = 10$ and rewiring probability $p \in \{0.05, 0.1, 0.15, \ldots, 1.0\}$ (p increasing from left to right). Circle area is proportional to the expected basin stability $\langle \bar{S}_{\mathcal{B}}\rangle$, and colour indicates the expected synchronizability $\langle R\rangle$. Squares represent real-world networks reported to exhibit a small-world topology (Supplementary Table S1). We chose ξ_L and ξ_C so that networks of different sizes can be compared with respect to average shortest path L and clustering coefficient C, quantities that characterize small-worldness[8]. $(\xi_L, \xi_C) = (0, 0)$ labels a regular network whereas $(\xi_L, \xi_C) = (1, 1)$ labels a random network. Small-world networks reside in the top-left quadrant. See Methods and Supplementary Information.

This adds a crucial piece to the puzzle and, we conjecture, makes its solution emerge (Fig. 4): in synchronizing networks, the functional need for the synchronous state to be as stable as possible promotes topological regularity. Thus, during network evolution, the optimization of synchronizability and the simultaneous optimization of basin stability have acted as two opposing forces. Their contest ended in a topological tradeoff: small-worldness.

Here, we have introduced basin stability, a new universal concept of stability. We see many important applications, notably cell regulatory networks, whose carcinogenic gene expression profiles have been related to cancer attractors in a high-dimensional multistable state space[28]. Like linear stability, basin stability is a property of a deterministic system and contains no information on the external perturbations that may affect it. Hence, it may often be promising to conceptually combine basin stability with a non-uniform distribution of perturbations. Basin stability could also be applied to stochastic systems by incorporating a suitable probabilistic notion of basins.

Methods

Estimation of basin stability in Watts–Strogatz networks of Rössler oscillators. A Watts–Strogatz network is constructed as follows[8]: starting from a one-dimensional ring of N nodes in which every node is connected to its k nearest neighbours, each edge is rewired independently with probability p by re-choosing one of its endpoints randomly. A Watts–Strogatz network generated with $p = 0$ ($p = 1$) has a regular (random) topology. An intermediate value of p yields a small-world topology.

In a given network, the dynamics at node i ($i = 1, \ldots, N$) are governed by the coupled Rössler equations (1)–(3). For $K \in I_s := (0.1232/\lambda_{\min}, 4.663/\lambda_{\max})$, we want to estimate the volume of the synchronous state's basin of attraction $\mathcal{B}$. High dimensionality poses challenges. If $\mathcal{B}$ were a bounded convex set, its volume could be estimated in $\mathcal{O}(n^4)$ time steps with today's best algorithm[29], where $n = 3N$ is the dimension of state space. We have $N \geq 100$, so this would be numerically very expensive. In any case, $\mathcal{B}$ is not convex in Rössler networks (see Supplementary Information). Thus, we retreat to something feasible: we estimate the volume of $\mathcal{B}$ in a relative sense, measuring basin stability as $S_{\mathcal{B}\cap\mathcal{Q}} = \mathrm{Vol}(\mathcal{B}\cap\mathcal{Q})/\mathrm{Vol}(\mathcal{Q}) \in [0, 1]$, where $\mathcal{Q}$ is a subset of state space that has finite volume.

More specifically, we integrate the system equations for T initial conditions drawn uniformly at random from $\mathcal{Q}$. We count the number M of initial conditions that arrive at the synchronous state (the other possible attractor being infinity) and estimate $S_{\mathcal{B}\cap\mathcal{Q}}$ as M/T. Observing that this is a repeated Bernoulli experiment, we infer that the estimate carries a standard error of

$$e := \frac{\sqrt{S_{\mathcal{B}\cap\mathcal{Q}}(1 - S_{\mathcal{B}\cap\mathcal{Q}})}}{\sqrt{T}}$$

At $T = 500$, for example, $e < 0.023$ in absolute terms.

In relative terms, $e < S_{\mathcal{B}\cap\mathcal{Q}}/10$ for $S_{\mathcal{B}\cap\mathcal{Q}} > 1/6$. $\mathcal{Q}$ should be chosen such that values of $S_{\mathcal{B}\cap\mathcal{Q}}$ typically surpass this level. Our choice underlying the results presented above is $\mathcal{Q} = q^N$ with $q = [-15, 15] \times [-15, 15] \times [-5, 35]$. Note that the Rössler attractor is included in q. We also studied other choices

of $\mathcal{Q}$—for instance $([-8,8]\times[-8,8]\times[-8,8])^N$—yet observed no qualitative difference in the outcomes. Therefore, we suppress the subscript $\mathcal{Q}$ when stating $S_{\mathcal{B}}$ in Fig. 3.

For each network in the ensemble, we estimate basin stability $S_{\mathcal{B}}$ for ten different equally spaced values $K \in I_s$ and average to obtain mean basin stability $\bar{S}_{\mathcal{B}}$.

The results are not qualitatively different for networks produced by a two-dimensional Watts–Strogatz model and another model that varies the link length distribution[30]. Details on this are provided in the Supplementary Information.

Topological comparison of small-world networks of different sizes. The axes of Fig. 4 were chosen so that different real-world networks can be compared, without the distorting effects of network size, with respect to average shortest path L and clustering coefficient C. L and C have been widely used to characterize small-worldness[8]. We plot ξ_L against ξ_C, where $\xi_X = 1-\log(X/X_{\mathrm{R}})/\log(X_{\mathrm{L}}/X_{\mathrm{R}})$ with $X = L$ or C. $L_{\mathrm{R}}, C_{\mathrm{R}}$ (or $L_{\mathrm{L}}, C_{\mathrm{L}}$) are the values of the respective quantities in random networks (or regular lattices) of the same size. ξ_X counts how many orders of magnitude X is away from X_{L} in relation to the count of orders of magnitude between X_{L} and X_{R}. This way $(\xi_L, \xi_C) = (0,0)$ labels a regular network whereas $(\xi_L, \xi_C) = (1,1)$ labels a random network. Small-world networks have[8] $L \approx L_{\mathrm{R}}$ and $C \gg C_{\mathrm{R}}$ and therefore reside in the top-left quadrant. See Supplementary Information.

Received 24 July 2012; accepted 22 November 2012; published online 6 January 2013

References

1. Babloyantz, A. & Destexhe, A. Low-dimensional chaos in an instance of epilepsy. *Proc. Natl. Acad. Sci. USA* **83,** 3513–3517 (1986).
2. Lytton, W. W. Computer modelling of epilepsy. *Nature Rev. Neurosci.* **9,** 626–637 (2008).
3. Machowski, J., Bialek, J. W. & Bumby, J. R. *Power System Dynamics: Stability and Control* (Wiley, 2008).
4. Erzgräber, H. *et al.* Mutually delay-coupled semiconductor lasers: Mode bifurcation scenarios. *Opt. Commun.* **255,** 286–296 (2005).
5. Da Silveira Lobo Sternberg, L. Savanna-forest hysteresis in the tropics. *Glob. Ecol. Biogeogr.* **10,** 369–378 (2001).
6. Hirota, M., Holmgren, M., Van Nes, E. H. & Scheffer, M. Global resilience of tropical forest and savanna to critical transitions. *Science* **334,** 232–235 (2011).
7. May, R. M. Thresholds and breakpoints in ecosystems with a multiplicity of stable states. *Nature* **269,** 471–477 (1977).
8. Watts, D. J. & Strogatz, S. H. Collective dynamics of 'small-world' networks. *Nature* **393,** 440–442 (1998).
9. Sporns, O. & Zwi, J. The small world of the cerebral cortex. *Neuroinformatics* **2,** 145–162 (2004).
10. Wang, Z., Scaglione, A. & Thomas, R. J. Generating statistically correct random topologies for testing smart grid communication and control networks. *IEEE Trans. Smart Grid* **1,** 28–39 (2010).
11. Pecora, L. M. & Carroll, T. L. Master stability functions for synchronized coupled systems. *Phys. Rev. Lett.* **80,** 2109–2112 (1998).
12. Barahona, M. & Pecora, L. M. Synchronization in small-world systems. *Phys. Rev. Lett.* **89,** 054101 (2002).
13. Hong, H., Kim, B. J., Choi, M. Y. & Park, H. Factors that predict better synchronizability on complex networks. *Phys. Rev. E* **69,** 067105 (2004).
14. Lenton, T. M. *et al.* Tipping elements in the earth's climate system. *Proc. Natl. Acad. Sci. USA* **105,** 1786–1793 (2008).
15. Nusse, H. E. & Yorke, J. A. Basins of attraction. *Science* **271,** 1376–1380 (1996).
16. Wiley, D. A., Strogatz, S. H. & Girvan, M. The size of the sync basin. *Chaos* **16,** 015103 (2006).
17. Scheffer, M. *et al.* Early-warning signals for critical transitions. *Nature* **461,** 53–59 (2009).
18. Van Nes, E. H. & Scheffer, M. Slow recovery from perturbations as a generic indicator of a nearby catastrophic shift. *Am. Nature* **169,** 738–747 (2007).
19. Holling, C. S. Resilience and stability of ecological systems. *Annu. Rev. Ecol. Syst.* **4,** 1–23 (1973).
20. Scheffer, M. *Critical Transitions in Nature and Society* (Princeton Univ. Press, 2009).
21. Boccaletti, S., Latora, V., Moreno, Y., Chavez, M. & Hwang, D-U. Complex networks: Structure and dynamics. *Phys. Rep.* **424,** 175–308 (2006).
22. Buldyrev, S. V., Parshani, R., Paul, G., Stanley, H. E. & Havlin, S. Catastrophic cascade of failures in interdependent networks. *Nature* **464,** 1025–1028 (2010).
23. Arenas, A., Díaz-Guilera, A., Kurths, J., Moreno, Y. & Zhou, C. Synchronization in complex networks. *Phys. Rep.* **469,** 93–153 (2008).
24. Fries, P. A mechanism for cognitive dynamics: neuronal communication through neuronal coherence. *Trends Cogn. Sci.* **9,** 474–480 (2005).
25. Fell, J. *et al.* Human memory formation is accompanied by rhinal-hippocampal coupling and decoupling. *Nature Neurosci.* **4,** 1259–1264 (2001).
26. Fell, J. & Axmacher, N. The role of phase synchronization in memory processes. *Nature Rev. Neurosci.* **12,** 105–118 (2011).
27. Hammond, C., Bergman, H. & Brown, P. Pathological synchronization in Parkinson's disease: Networks, models and treatments. *Trends Neurosci.* **30,** 357–364 (2007).
28. Huang, S. & Ingber, D.E. A non-genetic basis for cancer progression and metastasis: Self-organizing attractors in cell regulatory networks. *Breast Disease* **26,** 27–54 (2007).
29. Lovász, L. & Vempala, S. Simulated annealing in convex bodies and an $\mathcal{O}^*(n^4)$ volume algorithm. *J. Comput. Syst. Sci.* **72,** 392–417 (2006).
30. Li, G. *et al.* Towards design principles for optimal transport networks. *Phys. Rev. Lett.* **104,** 018701 (2010).

Acknowledgements

The authors acknowledge financial support from IRTG 1740 (Deutsche Forschungsgemeinschaft), the SUMO-project (European Union), the ECONS-project (Leibniz Association) and Konrad-Adenauer-Stiftung. They thank N. Fujiwara and A. Rammig for inspiring discussions.

Author contributions

P.J.M. conceived the study, performed the numerics, and prepared the manuscript. All authors discussed the results, drew conclusions and edited the manuscript. J.K. supervised the study.

Additional information

Supplementary information is available in the online version of the paper. Reprints and permissions information is available online at www.nature.com/reprints. Correspondence and requests for materials should be addressed to P.J.M.

Competing financial interests

The authors declare no competing financial interests.

nature physics
SUPPLEMENTARY INFORMATION
DOI: 10.1038/NPHYS2516

How basin stability complements the linear-stability paradigm

P. J. Menck, J. Heitzig, N. Marwan & J. Kurths

Here we present supplementary material that accompanies our paper *How Basin Stability Complements the Linear-Stability Paradigm*. The first section of the material contains a motivation of the conceptual model of Amazonian vegetation we use and a discussion of the mechanical damped driven pendulum. Both systems demonstrate that linear stability concepts are unreliable proxies of global stability. The second section contains details on our analysis of basin stability in synchronizing networks.

1 Linear Stability Fails at Indicating Global Stability

1.1 Conceptual Amazonian Vegetation Model

To motivate the simple growth equation that we use in the main text, we review the equilibrium model of Amazonian vegetation presented in ref. 5. Consider a region of the Amazon basin that is subdivided into cells having different dry season (d.s.) precipitation requirements for forest establishment. Assume that the frequency of cells whose d.s. precipitation requirement is p follows a normal distribution,

$$f(p) = \frac{1}{\sigma\sqrt{2\pi}}\, e^{-\frac{(p-\mu)^2}{2\sigma^2}}$$

with mean μ and standard deviation σ. Then the relative forest cover C in the region is related to the region's average d.s. precipitation P through

$$C(P) = \int_0^P f(p)dp. \tag{S1}$$

Forest cover increases overall precipitation because trees take up water stored in the soil and release it to the atmosphere via evapotranspiration. The total amount of d.s. precipitation in the region can therefore be expressed as

$$P(C) = P_{\text{in}} + C \cdot \Phi, \tag{S2}$$

where P_{in} is the precipitation inflow from other regions and Φ is the contribution of one unit of forest cover to overall precipitation. An arid region is characterized by low P_{in}.

Now imagine that the region has a certain level of forest cover C_{before} before global climatic climate change alters P_{in}. How will C change? A pictorial answer is given in Fig. S1.

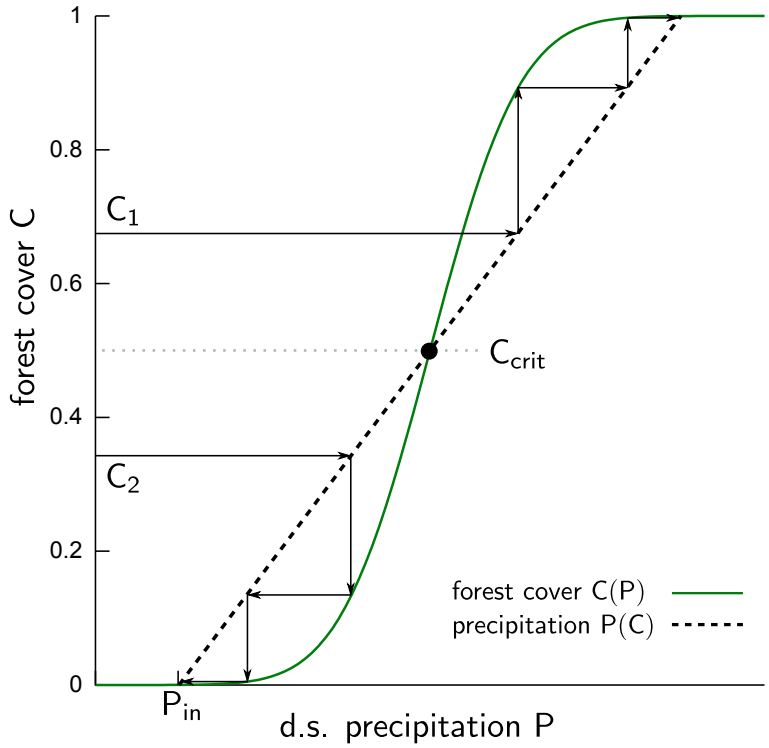

Supplementary Figure S1: **Equilibrium model of Amazonian vegetation.** The solid green line represents equilibrium forest cover C at d.s. precipitation P. The dashed black line is the overall d.s. precipitation P as a function of C. Step-stair sequences are shown for two different initial values of forest cover. Reproduced from ref. 5.

The solid green line represents equilibrium forest cover C at d.s. precipitation P, cf. eq. (S1). The dashed black line is the overall d.s. precipitation P at forest cover C, cf. eq. (S2). If $C_{\mathrm{before}} = C_1$, forest cover is above the critical threshold C_{crit}, so that P can support even more trees. Hence C grows, therefore P increases, upon which C grows further, and so on. Finally, due to this positive feedback loop, C is propelled towards 1.0. If, on the contrary, $C_{\mathrm{before}} = C_2$, forest cover is below C_{crit}. Forest cover at this level cannot be supported by P, starts to die back, again triggers a positive feedback loop, and eventually vanishes completely.

We describe the growth dynamics using the Levins model[31], a widely accepted basic vegetation model[32], to which we add a non-smooth switch in the growth term (corresponding to the limit $\sigma \ll \Phi$):

$$\frac{\mathrm{d}C}{\mathrm{d}t} = F(C) = \begin{cases} r(1-C)\,C - x\,C & \text{if} \quad C > C_{\mathrm{crit}}, \\ -x\,C & \text{if} \quad C < C_{\mathrm{crit}}. \end{cases}$$

According to this model, forest cover C grows with the saturating rate r if $C > C_{\mathrm{crit}}$ and dies with rate x (assuming $r > x > 0$). This model has two equilibria, the forest state $C_{\mathrm{F}} = 1 - \frac{x}{r}$ and the savanna state $C_{\mathrm{S}} = 0$. The equilibrium C_{F} (resp. C_{S}) exists and is stable if $C_{\mathrm{F}} > C_{\mathrm{crit}}$ (resp. $C_{\mathrm{crit}} > 0$). So, as in the equilibrium model reviewed above, C converges to a non-zero constant value if $C > C_{\mathrm{crit}}$ and vanishes completely otherwise. When increasing aridity drives up C_{crit}: i) C_{F}'s basin of attraction of shrinks, implying that C_{F} becomes less stable against perturbations such as strong deforestation (cf. Fig. 2). ii) C_{F} vanishes at $C_{\mathrm{crit}} = C_{\mathrm{F}}$.

Our model is conceptual. We do not intend it to serve as a description of reality. Rather, we use it as a reality-inspired aide to theory to illustrate the difference between the realm of small perturbations and the realm of non-small perturbations. This difference manifests itself in two phenomena:

i) As the linear stability coefficient of the forest state, $F'(C_{\mathrm{F}}) = x - r$, is a constant independent of C_{crit}, critical slowing down does not take place. This is reflected by a zero recovery exponent[33]. Indeed, critical slowing down may be absent in systems in which strong non-linearities such as switches exist.

ii) More important to us, because of their local nature, linear stability and the small-perturbation convergence rate do not sense that C_{F}'s basin of attraction of shrinks as C_{crit} goes up. The authors of ref. 34 write that "transitions caused by a sudden large disturbance without a preceding gradual loss of [stability against non-small perturbations][a] will not be announced by slowing down." On top of that, our model shows that slowing down may be absent *even if* such a gradual loss of stability is going on.

We conclude from this that linear stability and the small-perturbation convergence rate are *unreliable proxies* of how stable a state is against non-small perturbations. Instead of employing such local proxies, one should study global stability concepts like the one we suggest: basin stability.

The same conclusions can be drawn from the study of a basic damped driven pendulum (see next subsection).

[a]The original term they use is "resilience", refering to Holling's concept discussed in the main text.

1.2 Damped Driven Pendulum

Consider a classical damped pendulum driven by a constant angular acceleration T. Assume its dynamics to obey

$$\begin{aligned} \dot{\phi} &= \omega \\ \dot{\omega} &= -\alpha\omega + T - K\sin\phi, \end{aligned}$$

where $\alpha > 0$ is the dissipation coefficient and $K = g/\ell$, with the gravitational acceleration g and the pendulum's length ℓ.

In the following, we investigate the pendulum's solution space by varying $T \geq 0$ at fixed K, α ($T \leq 0$ reveals the mirror image). For $0 \leq T \leq K$, the pendulum has two fixed points $\mathbf{x}_i = (\phi_i, \omega_i)$, $i = 1, 2$, with coordinates

$$\begin{aligned} \phi_{1,2} &= \arcsin\left(\frac{T}{K}\right), \\ \omega_{1,2} &= 0 \end{aligned}$$

where we take ϕ_1 to be the solution of arcsin inside $[0, \pi/2]$ and $\phi_2 = \pi - \phi_1$. The eigenvalues of the Jacobian matrix at (ϕ_i, ω_i) read

$$\xi_i^{\pm} = -\frac{\alpha}{2} \pm \frac{\sqrt{\alpha^2 - 4K\cos\phi_i}}{2} \tag{S3}$$

and the maximum Lyapunov exponent of fixed point i is $\lambda_i = \mathrm{Re}\,\xi_i^{+}$. For $0 < T < K$, $\lambda_1 < 0$ and $\lambda_2 > 0$, because $\cos\phi_1 = -\cos\phi_2 > 0$. Hence the first fixed point $\mathbf{x}_1$ is a stable equilibrium and the second fixed point $\mathbf{x}_2$ is an unstable saddle. At $T = K$, a fold bifurcation occurs in which the two fixed points collide and disappear.

For $T > K$, the angular acceleration due to gravity cannot balance T and the pendu-

lum converges to a stable limit cycle in which ω oscillates around T/α. This limit cycle is also stable for a certain range $T_{\text{mult}} \leq T \leq K$. For these values of T, the pendulum is *multistable*. An example multistable state space is depicted in Supplementary Fig. S2.

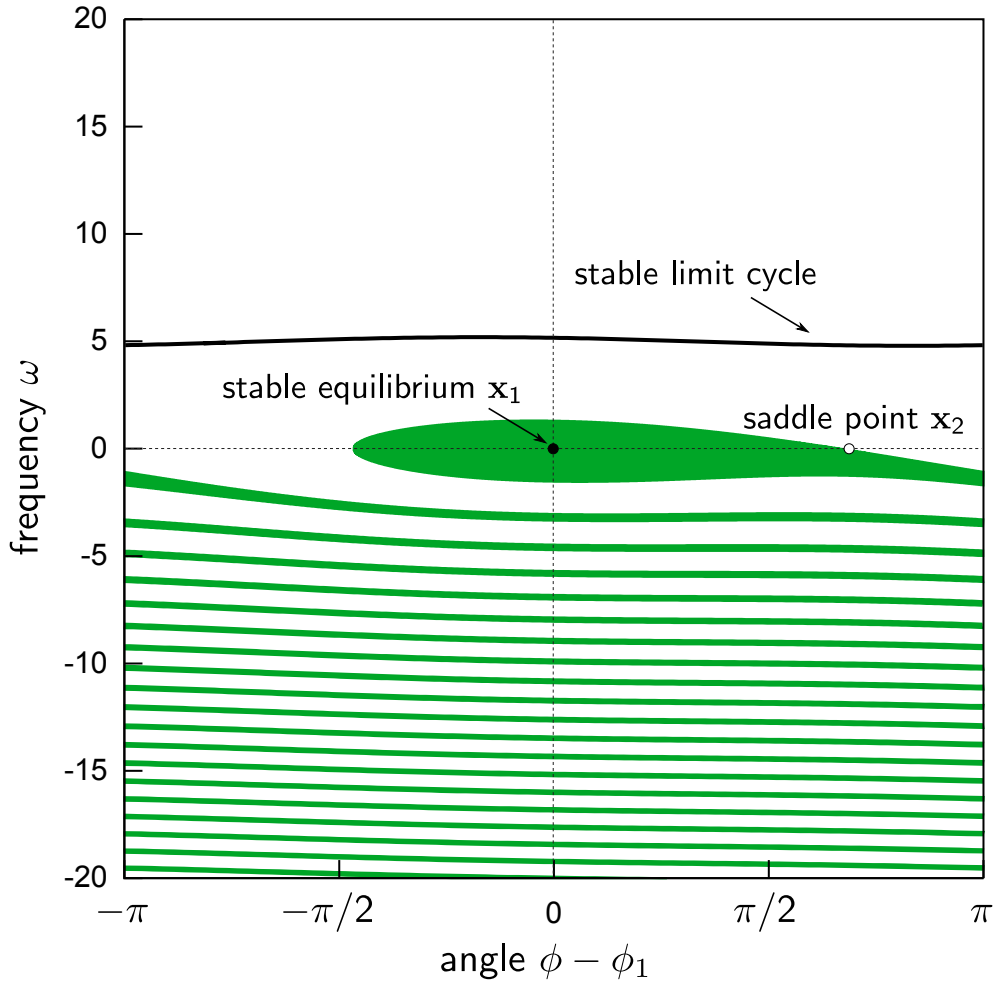

Supplementary Figure S2: **Phase Space of the Damped Driven Pendulum.** The filled (open) circle marks the stable equilibrium point $\mathbf{x}_1$ (the unstable saddle point $\mathbf{x}_2$). $\mathbf{x}_1$'s basin of attraction is indicated by the green area. From points in the non-coloured area, the pendulum converges to the limit cycle. We use $\alpha = 0.1$, $K = 1$, and $T = 0.5$.

For concreteness, we now choose $\alpha = 0.1$ and $K = 1$ and increase T from 0. First we look at linear stability. Supplementary Fig. S3 shows how the maximum Lyapunov

exponent λ_1 of the stable equilibrium $\mathbf{x}_1$ depends on T: Except very close to $T = 1$, λ_1 is *constant* and equal to $-\alpha/2$. Only at $T = 0.999997$, when the square root term contributing to the eigenvalues $\xi_1^{\pm}$ becomes real, does λ_1 start moving towards 0, where it reaches at $T = 1$.

Is critical slowing down, i.e., the decline of the small-perturbation convergence rate before the bifurcation, detectable *experimentally*? The maximum perturbation in positive ϕ-direction that the stable equilibrium $\mathbf{x}_1$ can withstand is $\phi_2 - \phi_1$ (cf. Supplementary Fig. S2), which at $T = 0.999997$ amounts to approximately $5 \cdot 10^{-3}$ rad $= 0.28°$. For a pendulum of length $\ell = 10$ cm, this corresponds to a displacement $\Delta = 0.5$ mm. Therefore, only if fluctuations induced by the environment are significantly less than Δ will critical slowing down be detectable in an experiment.

If critical slowing down is detectable, it occurs *very late* as T increases from 0 to 1. Hence critical slowing down appears not to be a reliable *early*-warning signal for the pendulum's critical transition.

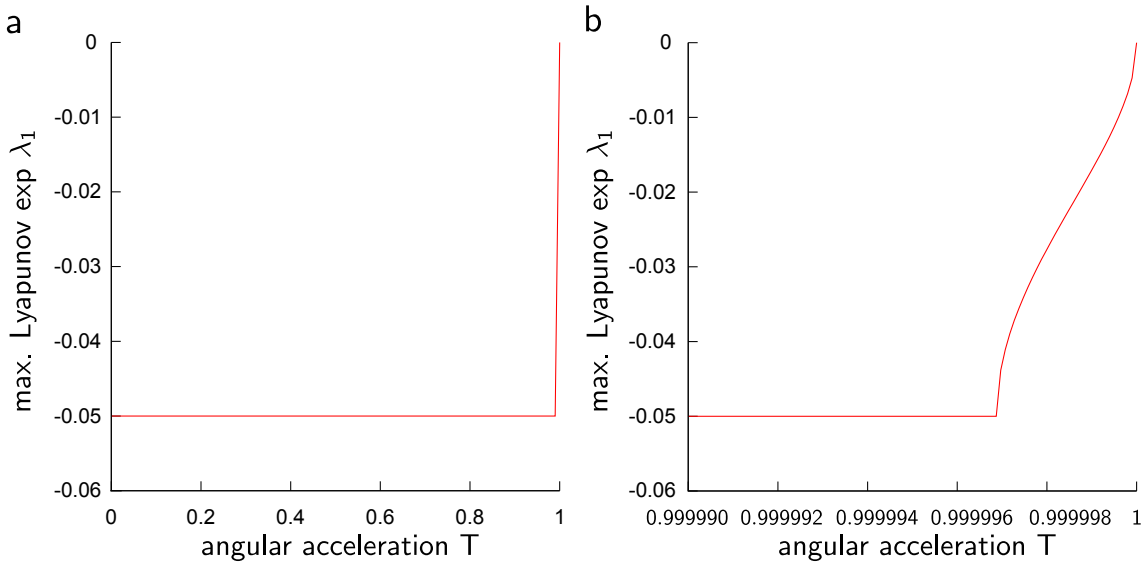

Supplementary Figure S3: **Linear Stability of the Damped Driven Pendulum. a,b:** Max. Lyapunov exp. λ_1 of the stable equilibrium versus T. **b** zooms in close to $T = 1$. We use $\alpha = 0.1$, $K = 1$.

Now we look at basin stability. To estimate $\mathbf{x}_1$'s basin stability $S_{\mathcal{B}}$, we randomly draw 1000 initial conditions from $[0, 2\pi] \times [-20, 20]$, integrate the system equations, and count in how many cases $\mathbf{x}_1$ (instead of the stable limit cycle) is reached. The result is shown in Supplementary Fig. S4. The limit cycle becomes stable at $T_{\text{mult}} \approx 0.13$. For $T \in [T_{\text{mult}}, 1)$, the pendulum is multistable. As T increases in this interval, basin stability $S_{\mathcal{B}}$ declines rapidly towards zero, where it reaches at $T = 1$.

None of this is indicated by the maximum Lyapunov exponent (cf. Supplementary Fig. S3a). Hence linear stability seems not to be a good proxy for the degree of stability against non-small perturbations.

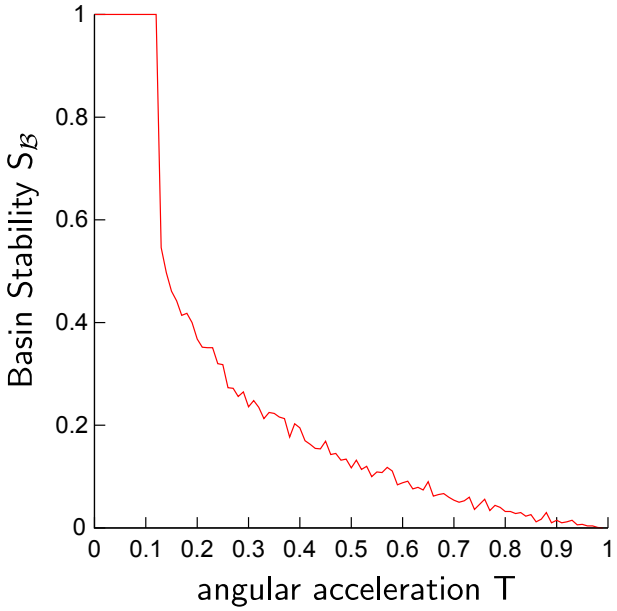

Supplementary Figure S4: **Basin Stability of the Damped Driven Pendulum.** Basin stability $S_{\mathcal{B}}$ of the stable equilibrium $\mathbf{x}_1$ versus T. We use $\alpha = 0.1$, $K = 1$.

2 Basin Stability in Synchronizing Networks

This section is ordered as follows. In the first subsection, we review the seminal study[11] by *Pecora and Carroll* on networks of identical oscillators that proposed the *Master Stability Function* (MSF) formalism and motivated the definition of *synchronizability*. In the second subsection, we elaborate on the computation of basin stability in Rössler networks. In the third subsection, we report properties of the real-world networks referred to in Fig. 4. The fourth subsection contains remarks about the non-convexity of the synchronous state's basin of attraction in Rössler networks.

2.1 Master Stability Function Formalism

Consider a system of N identical oscillators which are coupled through a connected network. Its dynamics are governed by the equations

$$\dot{\mathbf{r}}_i = \mathbf{F}(\mathbf{r}_i) + K \sum_j A_{ij}[\mathbf{H}(\mathbf{r}_j) - \mathbf{H}(\mathbf{r}_i)] = \mathbf{F}(\mathbf{r}_i) - K \sum_j L_{ij}\mathbf{H}(\mathbf{r}_j),$$

where $\mathbf{r}_i$ is the m-dimensional state vector describing the processes at node i. A is the adjacency matrix, with $A_{ij} = 1$ if there is an edge between nodes i and j and $A_{ij} = 0$ otherwise. $L_{ij} = \delta_{ij} \sum_k A_{ik} - A_{ij}$ is the Laplacian matrix with $\delta_{ij} = 1$ if $i = j$ and $\delta_{ij} = 0$ otherwise. Finally, K denotes the overall coupling constant and $\mathbf{H}(\mathbf{r})$ is the coupling function prescribing through which of their m components the connected nodes interact. $\mathbf{F}$ determines the evolution of each individual oscillator in the case of no coupling ($K = 0$). Because L_{ij} has zero row sum by definition, there always exists a synchronous state $\mathcal{M}_s = \{\mathbf{r}_1 = \mathbf{r}_2 = \ldots = \mathbf{r}_N = \mathbf{s}(t) | t \in \mathbb{R}\}$ in the Nm-dimensional state space in which all individual oscillators follow the same trajectory $\mathbf{s}(t)$. Technically, $\mathcal{M}_s$ is an invariant set of states rather than a state. However, for notational simplicity, we keep on calling it *the synchronous state.*

Is $\mathcal{M}_s$ stable? Based on linear stability, this problem was elegantly shown[11] to break up into two parts: Firstly, $\mathbf{F}, \mathbf{H}$ define a Master Stability Function $\mathrm{MSF}_{\mathbf{F},\mathbf{H}}$ that is independent of the network. Secondly, K and the network define a set of numbers at which $\mathrm{MSF}_{\mathbf{F},\mathbf{H}}$ has to be evaluated to find out whether $\mathcal{M}_s$ is stable. Indeed, $\mathcal{M}_s$ is stable if K and the eigenvalues $\lambda_1 = 0 < \lambda_2 \leq \ldots \leq \lambda_N$ of the positive semidefinite symmetric matrix L satisfy $\mathrm{MSF}_{\mathbf{F},\mathbf{H}}(K\lambda_i) < 0$ for all $i = 2, \ldots, N$. This condition is equivalent to demanding that all transverse eigenmodes of $\mathcal{M}_s$ have a negative Lyapunov exponent. Many choices of $\mathbf{F}$ and $\mathbf{H}$ yield a function $\mathrm{MSF}_{\mathbf{F},\mathbf{H}}$ that is negative only in an interval (α_1, α_2), so that $\mathcal{M}_s$ is stable if $\alpha_1 < K\lambda_i < \alpha_2$ for all $i = 2, \ldots, N$. This can only be fulfilled if $\lambda_N/\lambda_2 < \alpha_2/\alpha_1$, in which case the synchronous state is stable, provided K is chosen from the *stability interval* $I_s = (\alpha_1/\lambda_2, \alpha_2/\lambda_N)$. In the main text, $\lambda_2 =: \lambda_{\min}$, $\lambda_N =: \lambda_{\max}$, and $\beta = \alpha_2/\alpha_1$ is referred to as the *stability threshold*. Note that $\lambda_2 > 0$ if the network is connected as we have assumed here.

2.2 Basin Stability in Rössler networks

We study ensembles of Watts-Strogatz (WS) networks consisting of N Rössler oscillators that are coupled through their x-components. In each network, the dynamics of the oscillator at node i is determined by the equations

$$\begin{aligned} \dot{x}_i &= -y_i - z_i - K\sum_{j=1}^{N} L_{ij}x_j \\ \dot{y}_i &= x_i + ay_i \\ \dot{z}_i &= b + z_i(x_i - c) \end{aligned}$$

with $a = b = 0.2$ and $c = 7.0$. L is the network's Laplacian matrix and K is the overall coupling constant. We are interested in the stability of the synchronous state in which all oscillators follow the same trajectory on the Rössler attractor. According to the Master Stability Function formalism (see previous subsection), this state is stable if the network's synchronizability $R = \lambda_{\max}/\lambda_{\min}$ is lower than the threshold α_2/α_1, provided the coupling K is selected from the stability interval $I_s := (\alpha_1/\lambda_{\min}, \alpha_2/\lambda_{\max})$ (for x-coupled Rössler oscillators, $\alpha_1 = 0.1232$ and $\alpha_2 = 4.663$).

Fig. 3a displays that for ensemble networks with too small WS rewiring probability p the expected synchronizability $\langle R\rangle$ has not yet crossed α_2/α_1 so that the synchronous state is not stable (note the reversed y-axis in the Figure). But the expected synchronizability improves rapidly, soon passes the stability threshold, and then improves even further. However, the level of synchronizability just qualifies the synchronous state as stable or unstable. To quantify stability, we label by $S_{\mathcal{B}}$ the basin stability of the synchronous state. Being a relative measure of the basin's volume (see Methods), $S_{\mathcal{B}}$ is a number between 0 and 1. For each ensemble network we compute the mean basin stability $\bar{S}_{\mathcal{B}}$ by averaging over $S_{\mathcal{B}}(K)$ for several values of K within the stability interval. Strikingly, Figure 3b reveals that the expected mean basin stability $\langle\bar{S}_{\mathcal{B}}\rangle$ shows a behaviour opposite to that of

the expected synchronizability: After shooting up initially, expected mean basin stability $\langle \bar{S}_{\mathcal{B}} \rangle$ declines exponentially fast as the rewiring probability p increases. (This true for all choices of N and k that we analyzed, see Supplementary Fig.S5).

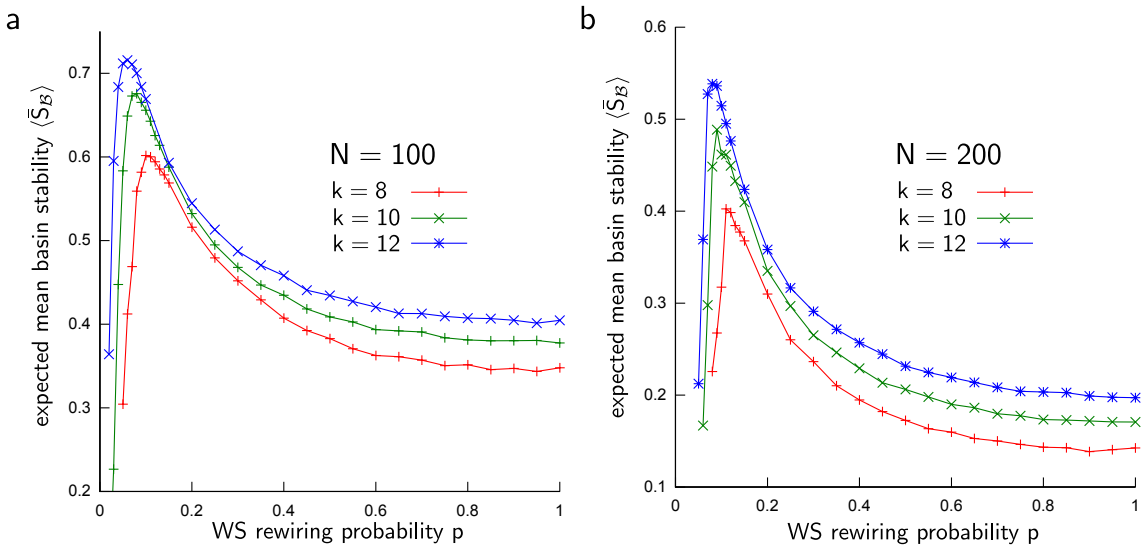

Supplementary Figure S5: **Basin Stability in Rössler networks.** Expected basin stability $\langle \bar{S}_{\mathcal{B}} \rangle$ versus p. Solid lines are guides to the eye. **a**: $N = 100$, **b**: N=200.

2.2.1 Qualitative Explanation

Why is this? Supplementary Fig. S6a displays that the expected basin stability $\langle S_{\mathcal{B}}(K)\rangle$ of a network at any fixed coupling K increases strongly as K grows and that it hardly depends on p. Hence a network's mean basin stability $\bar{S}_{\mathcal{B}}$ should be determined primarily by the location of its stability interval I_s. Indeed, for increasing p the expected stability interval $\langle I_s\rangle$ of a network significantly shifts to the left and simultaneously broadens (see Supplementary Fig. S6b). This qualitatively explains the rapidly decreasing behaviour of the expected mean basin stability shown in Fig. 3b. It also implies that the mean basin stability $\bar{S}_{\mathcal{B}}$ of a Rössler network mainly depends on the absolute values of $\lambda_{\min}$ and $\lambda_{\max}$ (which determine I_s), as opposed to their ratio which is central in synchronizability studies.

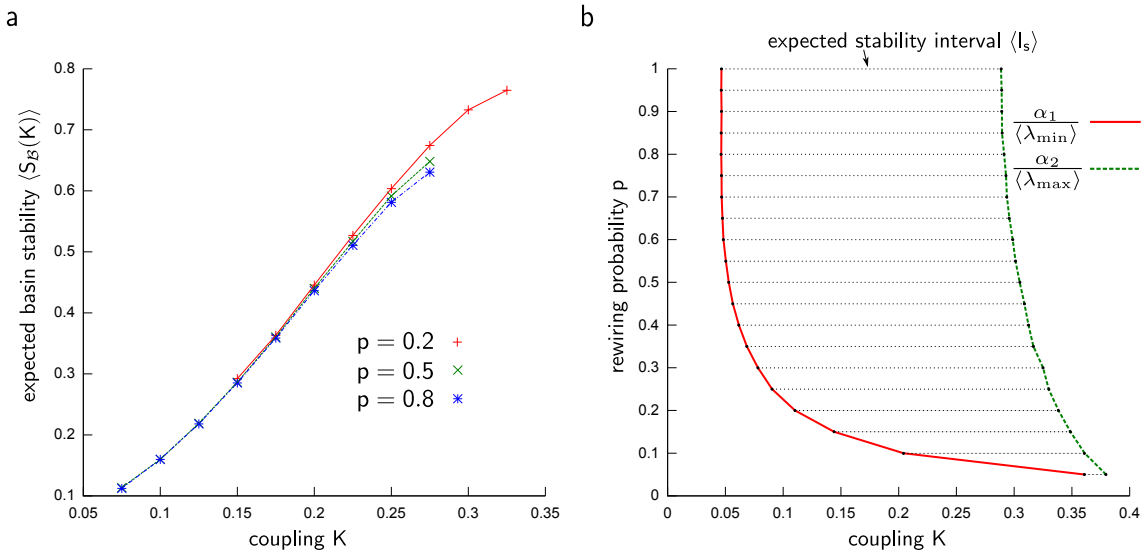

Supplementary Figure S6: **Explanatory characteristics.** **a**: expected basin stability $\langle S_{\mathcal{B}}(K)\rangle$ at coupling K, measured in the interior of the expected stability interval for $p = 0.2, 0.5, 0.8$. Solid lines are guides to the eye. **b**: expected stability interval $\langle I_s\rangle$ at rewiring probability p. The red solid line represents its left bound $\alpha_1/\langle\lambda_{\min}\rangle$, the green dashed line its right bound $\alpha_2/\langle\lambda_{\max}\rangle$.

2.2.2 Example Estimation of Mean Basin Stability $\bar{S}_{\mathcal{B}}$

For the sake of reproducibility, here we report the estimation of mean basin stability $\bar{S}_{\mathcal{B}}$ for an example network from the ensemble. Its edge list reads:

0-1	0-2	0-3	4-61	2-91	1-3	1-4	1-5	3-20	2-4	2-5	2-6	3-4	3-5	3-6	3-7
4-5	4-6	7-73	4-8	5-6	5-7	5-8	5-9	7-88	8-45	6-9	6-10	7-8	7-9	7-10	7-11
8-9	8-10	8-11	8-12	9-10	9-11	9-12	9-13	10-11	10-12	10-13	10-14	12-93	11-13	14-3	11-15
12-13	12-14	12-15	12-16	14-49	13-15	13-16	13-17	14-15	14-16	14-17	14-18	15-16	15-17	15-18	19-65
16-17	16-18	16-19	20-94	17-18	17-19	17-20	17-21	18-19	20-65	18-21	18-22	19-20	19-21	19-22	19-23
20-21	22-16	20-23	20-24	21-22	21-23	24-0	21-25	22-23	22-24	22-25	22-26	24-47	23-25	23-26	27-75
24-25	26-34	27-17	28-90	25-26	25-27	28-8	25-29	26-27	26-28	26-29	26-30	27-28	27-29	27-30	27-31
28-29	30-46	31-36	28-32	30-70	29-31	29-32	29-33	30-31	30-32	30-33	30-34	31-32	31-33	31-34	35-52
32-33	32-34	35-6	36-48	33-34	33-35	33-36	33-37	34-35	34-36	34-37	34-38	35-36	35-37	35-38	35-39
36-37	36-38	39-73	36-40	37-38	37-39	40-84	37-41	38-39	38-40	38-41	42-93	39-40	41-46	39-42	43-13
40-41	40-42	43-86	40-44	41-42	41-43	41-44	45-67	42-43	42-44	45-77	46-95	43-44	43-45	43-46	43-47
44-45	44-46	44-47	44-48	45-46	47-60	45-48	49-75	46-47	46-48	46-49	46-50	47-48	47-49	47-50	51-96
48-49	48-50	48-51	52-34	49-50	49-51	49-52	49-53	50-51	50-52	50-53	50-54	51-52	51-53	51-54	51-55
53-28	54-21	52-55	56-83	54-1	53-55	56-88	57-88	55-79	54-56	54-57	58-78	56-85	55-57	55-58	55-59
56-57	56-58	56-59	56-60	57-58	57-59	60-45	57-61	58-59	58-60	61-36	62-75	60-71	59-61	59-62	63-12
61-33	60-62	60-63	64-7	61-62	61-63	61-64	61-65	62-63	62-64	62-65	66-77	63-64	63-65	66-74	67-47
64-65	64-66	67-95	68-19	65-66	65-67	65-68	65-69	66-67	66-68	66-69	66-70	67-68	67-69	67-70	67-71
68-69	68-70	68-71	68-72	69-70	69-71	69-72	73-14	70-71	70-72	73-18	74-16	71-72	71-73	71-74	71-75
72-73	72-74	72-75	72-76	74-47	73-75	73-76	77-56	75-10	74-76	74-77	74-78	75-76	75-77	75-78	75-79
77-10	76-78	79-97	76-80	77-78	77-79	77-80	77-81	78-79	78-80	81-93	78-82	79-80	79-81	79-82	79-83
80-81	80-82	83-30	80-84	81-82	81-83	84-14	81-85	82-83	82-84	82-85	86-52	84-50	83-85	83-86	83-87
85-51	86-72	84-87	84-88	85-86	85-87	85-88	85-89	86-87	86-88	86-89	86-90	87-88	87-89	87-90	91-12
88-89	88-90	88-91	88-92	90-97	91-25	89-92	89-93	91-10	92-65	90-93	90-94	92-54	91-93	94-15	91-95
92-93	92-94	92-95	92-96	93-94	93-95	93-96	93-97	95-18	94-96	94-97	94-98	95-96	95-97	95-98	99-59
96-97	96-98	96-99	0-34	98-60	97-99	97-0	97-1	98-99	98-0	98-1	98-2	99-0	99-1	99-2	99-3

This network consists of $N = 100$ nodes and $E = 400$ edges (and was generated using the Watts-Strogatz model with rewiring probability $p = 0.2$). The minimum and maximum non-zero eigenvalues of its Laplacian matrix are $\lambda_{\min} = 1.236$ and $\lambda_{\max} = 13.87125$, respectively. Hence its stability interval $I_s = (0.010, 0.336)$. The synchronous state is stable for $K \in I_s$. We measure its basin stability at 11 different equally spaced values of K in the interior of I_s, namely 0.119, 0.139, 0.159, 0.179, 0.198, 0.218, 0.238, 0.258, 0.278, 0.297, 0.317, and obtain the corresponding sequence of $S_{\mathcal{B}}$-values: 0.226, 0.274, 0.330, 0.346, 0.472, 0.496, 0.594, 0.628, 0.656, 0.694, 0.690. To estimate the mean basin stability $\bar{S}_{\mathcal{B}}$ of this network, we compute the average of these values and obtain $\bar{S}_{\mathcal{B}} \approx 0.49$.

2.2.3 2-dimensional Watts-Strogatz Networks

In the main text and in the preceding sections of this supplementary material, we use a 1-dimensional ring as the initial configuration of the Watts-Strogatz algorithm. Here, we use the 2-dimensional lattice depicted in Supplementary Fig. S7.

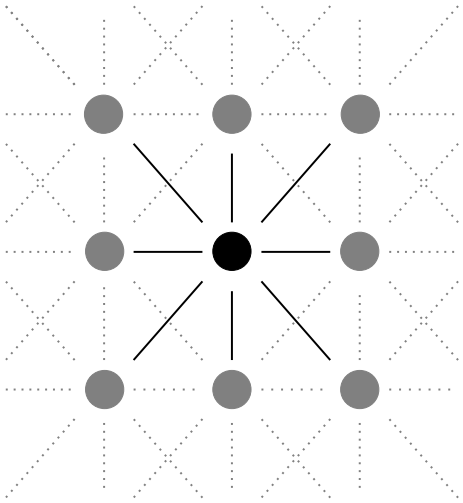

Figure S7: **Initial grid for 2-dimensional Watts-Strogatz (WS) network generation.** Each node is connected to its four nearest neighbours and the four diagonal ones among its next-nearest neighbours. So each node has 8 links.

We choose $N = 20 \cdot 20 = 400$ as the network size and, as before, place a Rössler oscillator at each node. Note that basin stability calculations on this lattice size approach the limits of what is computationally feasible today. For each network in the ensemble we estimate the basin stability $S_{\mathcal{B}}(K)$ for several $K \in I_s$ and compute their mean $\bar{S}_{\mathcal{B}}$. Here, we use a slightly smaller reference subset, $\mathcal{Q} = q^N$ with $q = [-15, 15] \times [-15, 15] \times [-4, 35]$, than above as otherwise the values of $S_{\mathcal{B}}$ are too small to be accuractely measurable with $T = 500$ integrations (cf. Methods). Note that the Rössler attractor is still included in q. Finally, we average $\bar{S}_{\mathcal{B}}$ over the ensemble to obtain $\langle \bar{S}_{\mathcal{B}} \rangle$.

The results are shown in Supplementary Fig. S8. There is no qualitative difference to Fig. 3: Whereas synchronizability improves as networks become more random, expected

basin stability is larger in networks that are more regular and falls off exponentially with increasing randomness.

Supplementary Fig. S9 shows how the 2-dimensional results compare topologically to synchronizing networks from the real-world (cf. Fig. 4). Again, there is no qualitative difference. Whereas the need for good synchronizability drives networks towards randomness, the need for large basin stability drives them towards regularity.

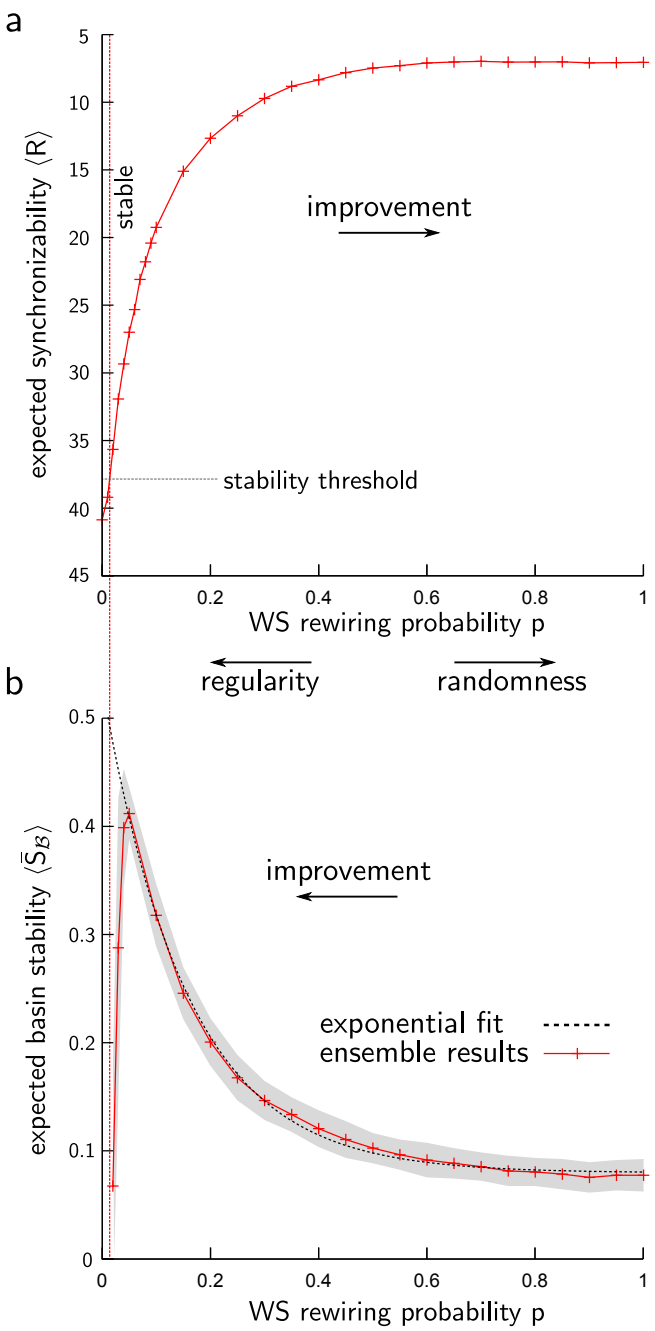

Figure S8: **Synchronizability and basin stability in 2-dimensional Watts-Strogatz (WS) networks of chaotic oscillators.** **a**: Expected synchronizability $\langle R \rangle$ versus the WS model's parameter p. The scale of the y-axis was reversed to indicate improvement upon increase in p. **b**: Expected basin stability $\langle \bar{S}_{\mathcal{B}} \rangle$ versus p. The grey shade indicates $\pm$ one standard deviation. The dashed line shows an exponential fitted to the ensemble results for $p \geq 0.05$. Solid lines are guides to the eye. The plots shown were obtained for $N = 400$ oscillators of Rössler type, each having on average $k = 8$ neighbours.

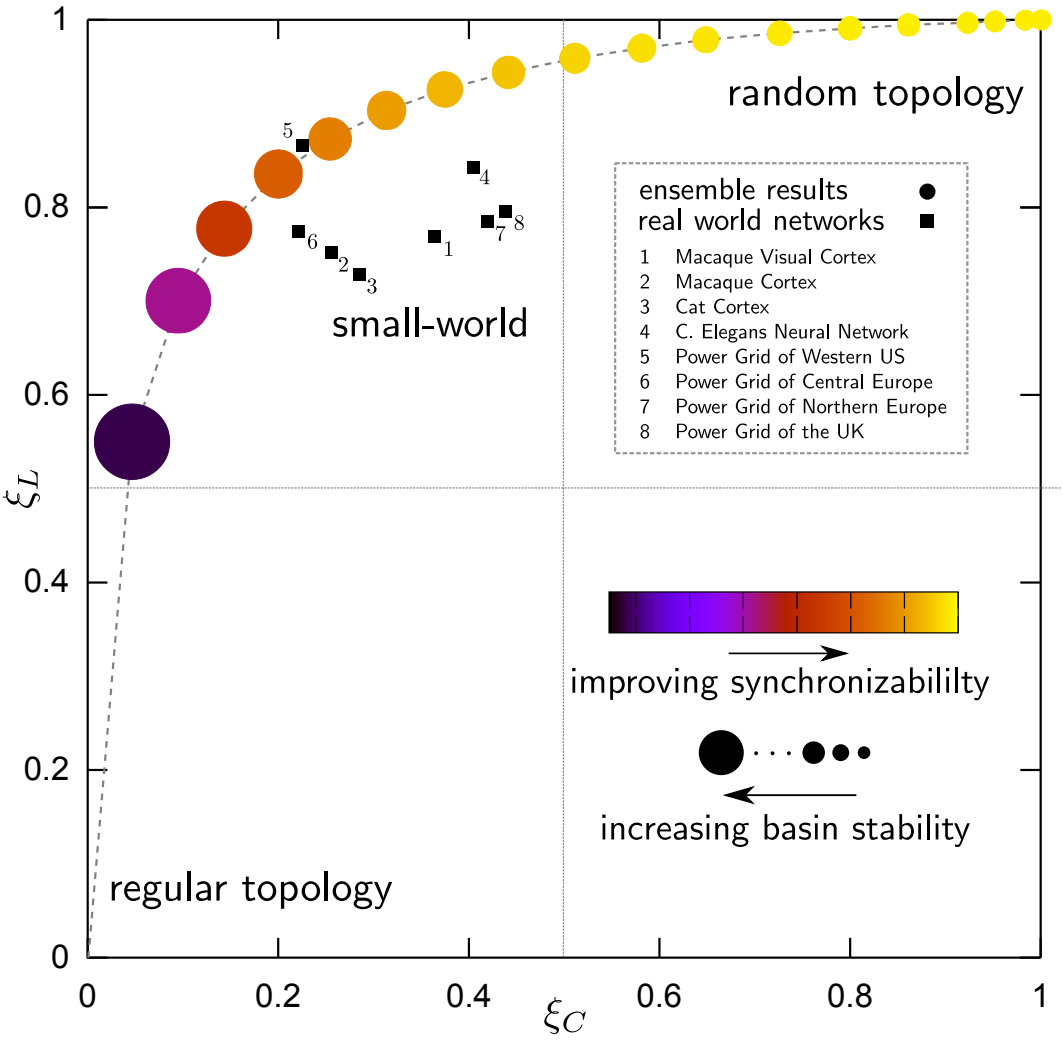

Figure S9: **Topological comparison of results for the 2-dimensional ensemble with real-world networks.** A circle represents the results for 2D Watts-Strogatz networks with $N = 400$, $k = 8$ and rewiring probability $p \in \{0.05, 0.1, 0.15, \ldots, 1.0\}$ (p increasing from left to right). A circle's area is proportional to the expected basin stability $\langle \bar{S}_{\mathcal{B}} \rangle$. A circle's colour indicates the expected synchronizability $\langle R \rangle$. Squares represent real-world networks reported to display a small-world topology (Supplementary Table 1). We chose ξ_L and ξ_C so that networks of different sizes can be compared w.r.t. average shortest path L and clustering coefficient C, quantities that characterize small-worldness[8]. $(\xi_L, \xi_C) = (0, 0)$ labels a regular network whereas $(\xi_L, \xi_C) = (1, 1)$ labels a random network. Small-world networks reside in the top left quadrant. See next section for details on the ξ_X, $X = L$ or C.

2.2.4 Small-World Networks with Different Link Length Distributions

Here we study small-world networks with different link length distributions. The networks are created as follows: We start with a 2-dimensional lattice in which every node is connected to its 4 nearest neighbours. Then we add short-cuts so that, in the end, the average number of links per node is 8. For short-cut addition, we use the following procedure[30]: A pair of nodes, (i, j) is chosen randomly. Then a new link connecting them is added to the network with probability

$$P(r) \propto r^{-\alpha},$$

where r is the Manhattan distance between i and j, i.e., the distance between them on the original 2-dimensional lattice with no short-cuts.

In networks created like this, we expect the length of a typical short-cut to decline when α increases. How do basin stability and synchronizability depend on α?

To investigate this, we choose the network size to be $N = 20 \cdot 20 = 400$ and, as before, place a Rössler oscillator at each node. Then for every network, we compute $\bar{S}_{\mathcal{B}}$. Here, we use a slightly smaller reference subset, $\mathcal{Q} = q^N$ with $q = [-15, 15] \times [-15, 15] \times [-3, 35]$, than above as otherwise the values of $S_{\mathcal{B}}$ are too small to be accuractely measurable with $T = 500$ integrations (cf. Methods). Note that the Rössler attractor is still included in q. Finally, we average $\bar{S}_{\mathcal{B}}$ over the ensemble to obtain $\langle \bar{S}_{\mathcal{B}} \rangle$.

Supplementary Fig. S10a shows that expected synchronizability $\langle R \rangle$ declines as α increases. This means that, from the linear stability perspective, an optimal link length distribution should fall off slowly or not at all (corresponding to rather low α).

The perspective of basin stability, again, disagrees with this. In Supplementary Fig. S10b, we see that $\langle \bar{S}_{\mathcal{B}} \rangle$ evolves in an opposite way to expected synchronizability in a large portion of the parameter interval: $\langle \bar{S}_{\mathcal{B}} \rangle$ grows as α increases. Finally, as α is tuned up further, basin stability reaches a maximum and then declines rapidly towards zero as synchronizability

approaches the stability threshold.

We think that these results do not contain considerably more information than Fig. 3 and Supplementary Fig. S8: For large α as well as for small p, networks have an intense local structure that is reduced as α decreases and p increases. This may be the common reason behind the phenomena we observe.

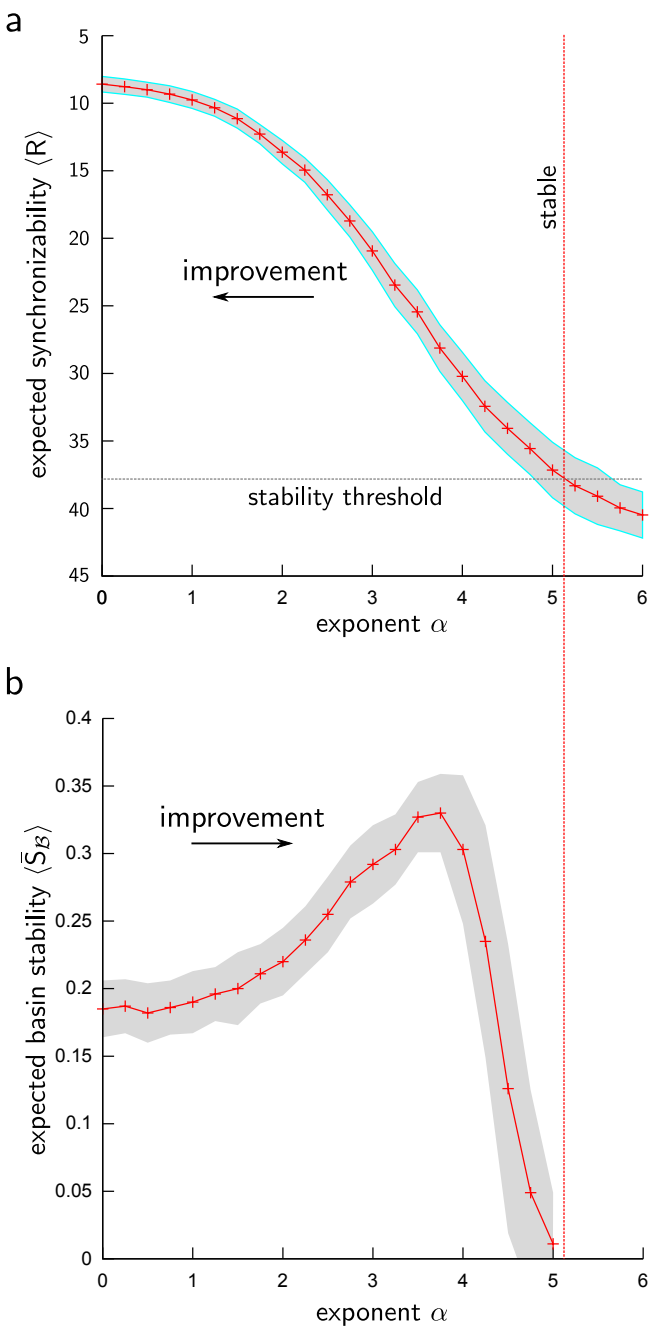

Figure S10: **Synchronizability and basin stability in networks of chaotic oscillators with different link length distribution. a**: Expected synchronizability $\langle R \rangle$ versus the link length distributions's parameter α. The scale of the y-axis was reversed. The grey shade indicates $\pm$ one standard deviation. **b**: Expected basin stability $\langle \bar{S}_{\mathcal{B}} \rangle$ versus α. The grey shade indicates $\pm$ one standard deviation. Solid lines are guides to the eye. The plots shown were obtained for $N = 400$ oscillators of Rössler type, each having on average $k = 8$ neighbours.

2.3 Properties of Studied Real-World Networks

Many synchronizing real-world networks were reported to display a small-world topology, among them neural networks and power grids[8,9]. We supply an overview of typical network properties for some such networks in Supplementary Table S1. Therein, L measures the average shortest path length between two vertices in the network and $C = \frac{1}{N}\sum C_i$ is the average of the nodal clustering coefficients

$$C_i = \frac{\sum_{j,k\in \mathsf{N}(i)} A_{jk}}{|\mathsf{N}(i)|^2 - |\mathsf{N}(i)|}.$$

In this formula, A is the adjacency matrix, $\mathsf{N}(i)$ is the set of nodes to which node i is linked, and $|\mathrm{N}(i)| = \sum_{j\in \mathsf{N}(i)} 1$ its cardinality[35].

A network is said to display a small-world topology if $C \gg C_\mathrm{R}$ and $L \approx L_\mathrm{R}$, where C_R and L_R are the average values of C and L in a random network that has the same number N of nodes and the same number E of edges[8]. To estimate C_R and L_R, we apply the Watts-Strogatz (WS) algorithm with rewiring probability $p = 1$ to regular ring lattices of given N and E and average over many realizations. The initial regular ring lattices are created in two steps. First, connect every node to its k nearest neighbours, where k is the largest even integer smaller than $\beta E/N$ with $\beta = 2$ ($\beta = 1$) for undirected (directed) networks. Second, add the remaining $E - kN/\beta$ edges randomly between nodes that are $k/2+1$ steps apart on the ring[9]. In Supplementary Table S1, beside C_R and L_R we report the averages C_L and L_L for lattice-like networks.

From the WS model's perspective, C and L assume their largest values in regular lattices and their lowest values in random graphs. Hence, small-world networks are rather similar to regular lattices w.r.t. C, yet at the same time rather similar to random graphs w.r.t. L. To quantify these similarities independently of the network size (as given by

N, E), we introduce

$$\xi_X = -\frac{\log(X/X_{\mathrm{L}})}{\log(X_{\mathrm{L}}/X_{\mathrm{R}})} = 1 - \frac{\log(X/X_{\mathrm{R}})}{\log(X_{\mathrm{L}}/X_{\mathrm{R}})}$$

with $X = L$ or C. ξ_X counts how many of orders of magnitude X is away from X_{L} in relation to the number of orders of magnitude between X_{L} and X_{R}. Note that $\log C$ can be interpreted as a measure of dimensionality[36]. Lattices have $\xi_C = \xi_L = 0$, whereas random graphs have $\xi_L = \xi_C = 1$. From the above, small-world networks should display ξ_C not too far from 0 and ξ_L not too far from 1 (and indeed the real networks studied here do so, see Fig. 4). We use ξ_C and ξ_L to topologically compare the networks listed in Supplementary Table S1 to the ensemble results on basin stability and synchronizability reported in the main text.

#	Network	N	E	C	L	C_{R}	L_{R}	C_{L}	L_{L}
1	Macaque Visual Cortex	30	311	0.53	1.73	0.36	1.66	0.66	1.93
2	Macaque Cortex	71	746	0.46	2.38	0.15	2.03	0.66	3.85
3	Cat Cortex	52	820	0.55	1.81	0.31	1.70	0.69	2.14
4	C. Elegans Neural Network	297	2345	0.18	3.99	0.027	2.98	0.64	19.25
5	Power Grid of Western US	4941	6594	0.08	18.99	0.00035	10.19	0.39	925.7
6	Power Grid of Central Europe	4335	5551	0.07	28.73	0.00020	10.73	0.35	846.8
7	Power Grid of Northern Europe	524	640	0.04	14.49	0.0030	8.38	0.29	107.6
8	Power Grid of the UK	393	484	0.04	12.54	0.0034	7.78	0.30	80.3

Supplementary Table S1: **Overview of properties of some real-world networks.** N specifies the number of nodes and E the number of edges in the network. Furthermore, L is the average shortest path length and C the clustering coefficient. These two quantities have been widely used to characterize small-worldness[8]. X_{R} (or X_{L}) represent average values of X computed in random networks (or lattices) of the same N, E, where $X = L, C$. For networks 1 to 3, the values of L and C were taken from ref. 9.

2.4 Non-Convexity of the Basin in Rössler-networks

Convexity of the basin $\mathcal{B}$ of the synchronous state in a network of Rössler oscillators would make the computation of its volume simpler. However, we clearly find that $\mathcal{B}$ is not convex. This follows from the non-convexity of the chaotic attractor's basin $\mathcal{B}_1$ of a single Rössler oscillator, as obvious from the two-dimensional details displayed in Supplementary Fig. S11. $\mathcal{B}_1^N := \{\mathbf{r}_1 = \ldots = \mathbf{r}_N = \mathbf{r} \mid \mathbf{r} \in \mathcal{B}_1\}$ is a subset of the synchronous state's basin $\mathcal{B}_N$ for every $N \geq 1$. Consequently, $\mathcal{B}_N$ is not convex either. Hence the powerful tools for volume estimation of convex bodies are not applicable here.

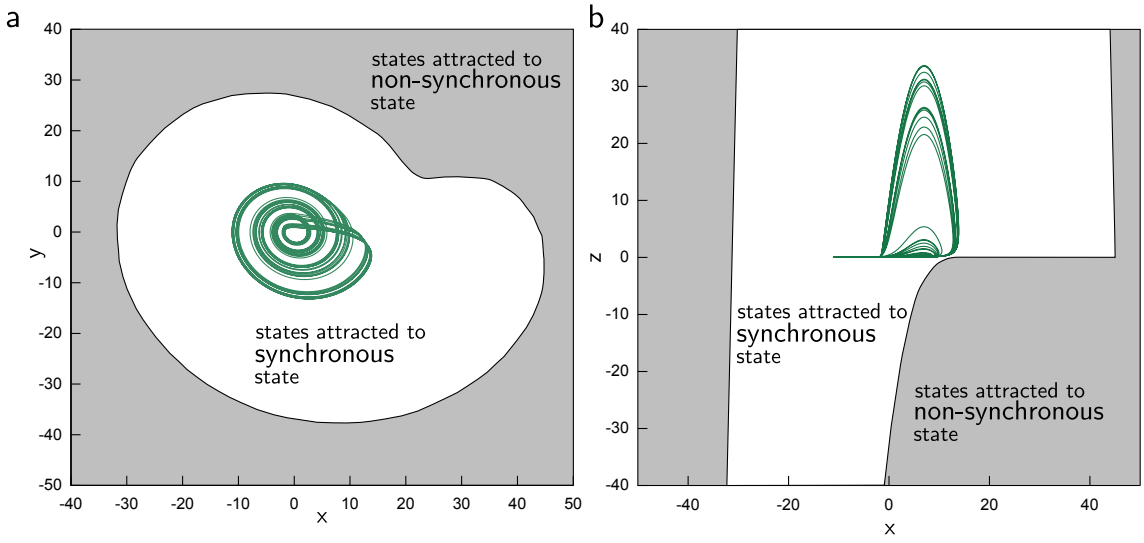

Supplementary Figure S11: **Two-dimensional details of the Rössler attractor's basin**. **a:** shows the xy-detail. A point (x, y) refers to the initial state $(x, y, 0)$. **b:** shows the xz-detail. A point (x, z) refers to the initial state $(x, 0, z)$. In both panels the white region indicates the Rössler attractor's basin of attraction. The green shape depicts a two-dimensional projection of the Rössler attractor.

References

[31] Levins, R. Some demographic and genetic consequences of environmental heterogeneity for biological control. *Bull. Entomol. Soc. Am.* **15**, 237–240 (1969).

[32] Tilman, D. Competition and biodiversity in spatially structured habitats. *Ecology* **75**, 2–16 (1994).

[33] Kuehn, C. A mathematical framework for critical transitions: Bifurcations, fastslow systems and stochastic dynamics. *Physica D* **240**, 1020 – 1035 (2011).

[34] Dakos, V., Scheffer, M., van Nes, E.H., Brovkin, V., Petoukhov, V. & Held, H. Slowing down as an early warning signal for abrupt climate change. *Proc. Natl. Acad. Sci. USA* **105**, 14308–14312 (2008).

[35] Newman, M.E.J. The structure and function of complex networks. *SIAM Rev.* **45**, 167–256 (2003).

[36] Donner, R.V., Heitzig, J., Donges, J.F., Zou, Y., Marwan, N. & Kurths, J. The geometry of chaotic dynamics – a complex network perspective. *Eur. Phys. J. B* **85**, 653 – 672 (2011).